A *Myo7a* mutation cosegregates with stereocilia defects and low-frequency hearing impairment

Charlotte R. Rhodes,[1]⋆ Ronna Hertzano,[2]⋆ Helmut Fuchs,[3] Rachel E. Bell,[2] Martin Hrabé de Angelis,[3] Karen P. Steel,[1] Karen B. Avraham[2]

[1]MRC Institute of Hearing Research, University Park, Nottingham, NG7 2RD, UK
[2]Department of Human Genetics and Molecular Medicine, Sackler School of Medicine, Tel Aviv University, Tel Aviv, Israel
[3]GSF Research Center for Environment and Health, Institute of Experimental Genetics, Neuherberg, Germany

Abstract

A phenotype-driven approach was adopted in the mouse to identify molecules involved in ear development and function. Mutant mice were obtained using *N*-ethyl-*N*-nitrosourea (ENU) mutagenesis and were screened for dominant mutations that affect hearing and/or balance. Heterozygote headbanger (*Hdb*/+) mutants display classic behavior indicative of vestibular dysfunction including hyperactivity and head bobbing, and they show a Preyer reflex in response to sound but have raised cochlear thresholds especially at low frequencies. Scanning electron microscopy of the surface of the organ of Corti revealed abnormal stereocilia bundle development from an early age that was more severe in the apex than the base. Utricular stereocilia were long, thin, and wispy. Homozygotes showed a similar but more severe phenotype. The headbanger mutation has been mapped to a 1.5-cM region on mouse Chromosome 7 in the region of the unconventional myosin gene *Myo7a*, and mutation screening revealed an A>T transversion that is predicted to cause an isoleucine-to-phenylalanine amino acid substitution (I178F) in a conserved region in the motor-encoding domain of the gene. Protein analysis revealed reduced levels of myosin VIIa expression in inner ears of headbanger mice. Headbanger represents a novel inner ear phenotype and provides a potential model for low-frequency-type human hearing loss.

⋆These authors contributed equally to this study.

Correspondence to: K.P. Steel, The Wellcome Trust Sanger Institute, Wellcome Trust Genome Campus, Hinxton, Cambridge, CB10 1SA, UK; E-mail: kps@sanger.ac.uk

N-ethyl-*N*-nitrosourea (ENU) mutagenesis screens are providing new mouse models for human hearing impairment, a requisite for studying the complexity of inner ear development (Erven et al. 2002; Vreugde et al. 2002; Curtin et al. 2003). The six sensory regions in the mammalian inner ear are composed of a mosaic of mechanosensory hair cells and supporting cells. An important defining feature of the hair cells is their array of actin-filled stereocilia that project from their apical surface. These structures play a fundamental role in the process of mechanotransduction that is initiated by the deflection of the stereocilia bundle as a result of fluid movement in the inner ear. The stereocilia bundles in the mammalian ear have very precise dimensions depending on the type of hair cell and the region of the cochlea. Indeed, the organ of Corti is tonotopically organized such that the apical hair cells are sensitive to low frequencies and the basal hair cells are most sensitive to high frequencies. The formation of the stereocilia bundle has been studied in detail in hamster and in chick (Tilney et al. 1992; Kaltenbach et al. 1994). Currently we know relatively little about the molecules involved in hair cell development but the mouse is proving to be a valuable asset in overcoming this deficit.

Positional cloning and the analysis of genetically modified mice have identified several genes that affect the maintenance and integrity of the hair cell stereocilia bundle. For example, mutations in *Cdh23* and *Pcdh15* cause disorganization of stereocilia in waltzer and Ames waltzer mice (Alagramam et al. 2001; Di Palma et al. 2001), respectively, and mutations in the human *CDH23* and *PCDH15* genes are responsible for Usher syndromes type 1D and 1F in humans (Ahmed et al. 2001; Bolz et al. 2001). In addition, several unconventional myosin molecules have been identified that also are involved in stereocilia development and/

or maintenance in mice. These include *Myo6* (Snell's waltzer), *Myo15* (shaker2), and *Myo7a* (shaker1). Mutations in these genes lead to stereocilia fusion, short stereocilia, and disorganized stereocilia, respectively (Probst et al. 1998; Self et al. 1998, 1999).

Shaker1 mice carry a recessive mutation in *Myo7a* and the equivalent human gene, *MYO7A*, is involved in Usher syndrome 1B in humans, in which congenital balance and hearing defects are accompanied by progressive retinitis pigmentosa (Weil et al. 1995; Weston et al. 1996; Levy et al. 1997; Liu et al. 1997a,b). The stereocilia in shaker1 mice become progressively disorganized and are found grouped together in clumps rather than the classic V or W shape (Self et al. 1998). By postnatal day (P) 20 many hair cells have degenerated. This hair cell anomaly is believed to be responsible for their abnormal behavior that is indicative of vestibular dysfunction. The present study shows that the stereocilia of headbanger mice are abnormal. However, their phenotype differs from that of shaker1 mice. Outer hair cell stereocilia form O shapes in contrast to the normal V shape. In addition, many inner hair cell stereocilia fuse and elongate forming giant stereocilia, which are not seen in wild-type cochleae. A predicted amino acid substitution in myosin VIIa was identified in headbanger mutants, which may be associated with their hair cell pathology.

Materials and methods

Mice. The founder mouse carrying the dominant *Hdb* mutation was generated in a large-scale ENU mutagenesis program in Neuherberg (Hrabé de Angelis et al. 2000). Male C3HeB/FeJ mice were mutagenized and mated to normal C3HeB/FeJ females and the F1 offspring were screened for a variety of defects, including deafness and vestibular dysfunction. The *Hdb* founder was identified because of head bobbing and hyperactivity. The shaker1 (*Myo7a^{4626SB}*) mice were generated by ENU mutagenesis of BALB/c males and were repeatedly backcrossed to a BS inbred strain; they were kindly provided by Oak Ridge National Laboratories (Oak Ridge, TN). They have since been crossed onto a CBA/Ca inbred strain and are thus maintained on a 50% CBA/Ca, 50% BS, and some BALB/c genetic background. All experiments were carried out in full compliance with the Tel Aviv University Animal Care and Use Committee (M-03-58) and UK Home Office regulations.

Scanning electron microscopy (SEM). Samples (E18.5 +/+ n = 9, *Hdb*/+ n = 9; P1 +/+ n = 8, *Hdb*/+ n = 8; P20 +/+ n = 9, *Hdb*/+ n = 14; *Hdb*/*Hdb* n = 4; 3 months +/+ n = 9, *Hdb*/+ n = 3; *Hdb*/*Hdb* n = 3) were fixed in 2.5% glutaraldehyde in 0.1 M phosphate buffer and then prepared using the osmium tetroxide-thiocarbohydrazide (OTOTO) method as described previously (Self et al. 1998). After critical point drying and gold coating with a thin layer of gold, the samples were analyzed using a Philips XL30 SEM at 10 kV. For hair cell counts, montages were made from the apex (80%–100% of the length of the cochlear duct from the base) of the cochlea covering between 500 and 800 μm for each region of each cochlea analyzed. Hair cell counts were compared by the Student's *t*-test using a significance level of $p < 0.01$.

Paint filling. Paint fills were carried out essentially as described (Martin and Swanson 1993). Heads of wild-type and *Hdb* mice (E16.5 +/+ n = 12, *Hdb*/+ n = 15; P3 +/+ n = 14, *Hdb*/+ n = 5, *Hdb*/*Hdb* n = 4; P20 +/+ n = 8, *Hdb*/+ n = 10) were removed and then fixed in Bodians fixative (75% ethanol, 5% formalin, 5% glacial acetic acid) overnight followed by washing (minimum 2 h for each wash) twice in each of the following solutions: 75% ethanol, 95% ethanol, 100% ethanol. The heads were bisected and cleared overnight in methyl salicylate. The endolymphatic compartment of the inner ears was injected via the common crus and the cochlea employing a pulled glass capillary pipette (20–40-μm diameter) filled with 1% gloss paint in methyl salicylate. Finally, we dissected the ears free of the skull and photographed them in methyl salicylate using an Olympus DP10 digital camera.

Mapping and sequence analysis. *Hdb*/+ mice on their C3HeB/FeJ background were outcrossed to C57BL/6J mice and the mutant progeny were backcrossed to C57BL/6J. This produced a total of 282 N2 backcross mice, 71 of which exhibited a mutant phenotype. Mouse tail DNA was extracted from clearly mutant animals phenotyped independently by two people. Only mice swimming in circles or unable to swim at all in addition to the head bobbing and hyperactive behavior were counted as mutants. A low-resolution genome scan was performed by typing the first 47 mice for a panel of 59 microsatellite markers (Kiernan et al. 1999) polymorphic between the two strains C3HeB/FeJ and C57BL/6J. Once a region of linkage on Chromosome 7 was identified, we extended the Chromosome 7 analysis to all mutant mice and refined the map position by typing N2 recombinant mice for additional microsatellite polymorphic markers or identified polymorphic SNPs within the linkage interval. We carried out a mutation analysis by direct sequencing of PCR products of the following genes: p21/cdc42/

rac1 activated kinase 1 (*Pak1*), wingless-related MMTV integration site 11 (*Wnt11*), and myosin VIIa (*Myo7a*). Testes RNA was extracted and cDNA was reverse-transcribed as described (Donaudy et al. 2003). Primer sequences are available upon request.

Bioinformatics analysis. A 3D model of the head–motor domain of the mouse myosin VIIa protein (SwissProt code: MY7A_MOUSE) was obtained using the experimentally determined structure of *Dictyostelium discoideum* myosin IE as a template (Kollmar et al. 2002) (PDB code: 1LKX, chain C). The homology model building was carried out using a pairwise alignment of these two proteins and the NEST facility of the Jackal protein structure modeling package (http://trantor.bioc.columbia.edu/programs/jackal/index.html). Residue conservation scores, calculated using a multiple sequence alignment (MSA) of 75 myosin homologs, were colorcoded onto the model of myosin VIIa. ConSurf [http://consurf.tau.ac.il/ (Glaser et al. 2003)] color codes the amino acid conservation grades and projects them onto the structure.

Genotyping. A mutation was identified in *Myo7a* that adds a recognition site for the restriction enzyme *Eco*571. However, an additional recognition site for this enzyme lies in the intronic sequence flanking the mutation, making it unsuitable for genotyping. *Xcm*I has a bipartite restriction enzyme recognition site that at one end solely matches with the wild-type sequence of the headbanger mutation. Primers were designed to artificially introduce the second restriction enzyme site within the PCR product (underlined). Genomic DNA was amplified using the forward primer 5′ GAA GAC TCG ATC TAT TGT AAC AAC TGC 3′ and the reverse primer 5′ TGC TCG ATC CAT GAG TCC AGT CCA CTG 3′. Digesting PCR products with *Xcm*I cuts the wild-type DNA only and generates a single band of 172 bp for homozygote mutants, two bands for heterozygote animals at 172 and 148 bp, and a single band at 148 bp for wild-type animals.

A complementation test was performed between *Hdb*/+ and *sh1/sh1* mutant mice (*Myo7a*[4626SB]). The progeny from this test were genotyped for the *Hdb* allele as described above, and for the *Myo7a*[4626SB] allele by PCR as described previously (Holme and Steel 2002).

Auditory physiology. Mice (P20–23 +/+ *n* = 6, *Hdb*/+ *n* = 11, *Hdb*/*Hdb* *n* = 2) were anesthetized with urethane, the middle ear cavity was opened, and a recording electrode was placed on the round window of the cochlea (Steel and Smith 1992). Shaped tone burst stimuli of 15-ms duration, 1-ms rise/fall time with a 100-ms interstimulus interval, were delivered through a closed, calibrated sound system. Thresholds for detection of a cochlear nerve compound action potential (CAP) response were obtained in 2-dB steps. The endocochlear potentials were measured (P20–23 +/+ *n* = 6, *Hdb*/+ *n* = 11, *Hdb*/*Hdb* *n* = 2) with a micropipette electrode inserted into the basal turn scala media through the lateral cochlear wall. AH data are given as ±SEM.

Protein analysis. Mice from three separate litters were sacrificed at p4, cochleas were dissected out of the temporal bones in cold phosphate buffer saline while carefully separating the saccule from the cochlea, and snap frozen in 1.5-ml tubes in liquid nitrogen. DNA was extracted from the tail tips and mice were genotyped for the headbanger mutation, as described. From each litter, all three genotypes were selected; cochleas were placed in modified radioimmunoprecipitation (RIPA) lysis buffer and homogenized with a Kontes pellet pestle. After lysis and centrifugation, protein-loading amounts were equalized using a Bradford protein quantification assay. Samples were then separated on a 7.5% SDS–PAGE gel and transferred to a Hybond-P PVDF membrane (Amersham Biosciences). After blocking in Tris buffered saline with Tween (TBST) with 5% nonfat skim milk, membranes were cut and a Western blot was performed with the following antibodies: rabbit polyclonal antibodies for myosin VIIa (1:1000) and myosin VI (1:1000) and a monoclonal antitubulin (Sigma) (1:500,000). Densitometry was performed using the Liscap and TINA programs. Statistics for the myosin VIIa protein were done with a one-tailed *t*-test and with a two-tailed *t*-test for the myosin VI protein. The *t*-test was selected as each experiment compared between two data sets (wt–hom; wt–het; het–hom) and the variance is unknown although assumed as equal between samples. The *t*-test was unpaired.

For immunohistochemistry and confocal imaging, mice were sacrificed at P0–P1, organ of Corti were dissected out of the cochleae, cultured for 12–24 h (Kelley et al. 1993), and then fixed. Genotyping was performed as described above. Cultures were stained with rhodamine-phalloidin (red) to visualize the actin cytoskeleton; and-myosin VIIa (1:100) antibody with a secondary FITC conjugated antibody (green) to visualize the myosin VIIa protein.

Results

Stereocilia defects in heterozygote headbanger mutants (Hdb/+). SEM analysis of the surface of the organ of Corti of headbanger mutants revealed ab-
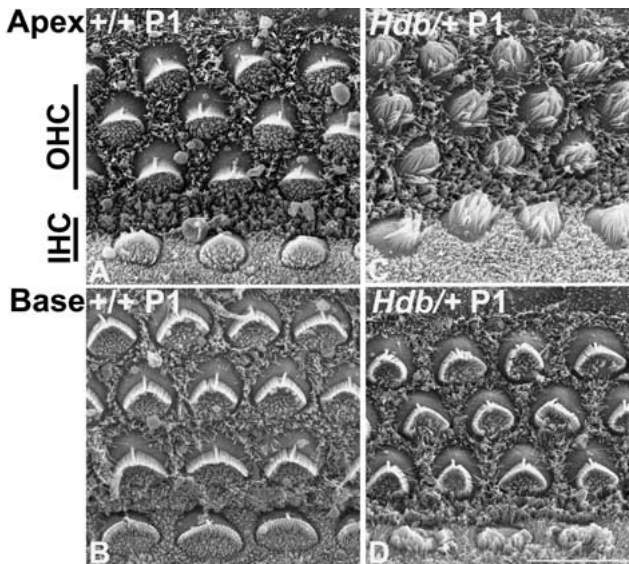
Fig. 1. Scanning electron micrographs taken from P1 control (**A**, **B**, +/+) and headbanger (**C**, **D**, *Hdb*/+) mutant animals. In the apical turn, stereocilia bundles of both IHCs and OHCs cover the whole apical hair cell surface and have not formed a polarized staircase array (**C**) as observed in the controls (**A**). In the basal turn, OHC stereocilia bundles do form a V-shaped staircase but with additional inward-pointing wings making them appear more U-shaped (**D**) and the IHC stereocilia are disorganized (**D**). Basal IHC stereocilia bundles (**D**) extend from the whole apical surface of the hair cell compared with the control (**B**). Scale bar = 10 μm.

normal stereocilia bundle formation predominantly in the apex of the cochlea. A range of ages was analyzed to gain a developmental time course of the pathology [from embryonic day (E) 18.5 to 3 months]. At E18.5, stereocilia bundles of both inner and outer hair cells (IHC and OHC, respectively) extended from the apical surface of the hair cell with no clear height gradient in the *Hdb*/+ mutants compared with the controls in the apical turn (data not shown). In controls, the developing stereocilia bundles migrate to one pole of the cell and form a staircase-like pattern of graded heights. This process appears to be affected in *Hdb*/+ mutants. OHC stereocilia in the base appeared similar to wild-type cochleae but the IHC stereocilia bundles were disorganized and appeared similar to the apical IHC stereocilia bundles. By P1 a similar phenotype to that seen at E18.5 was observed in both apical IHCs and OHCs (Fig. 1). However, in the basal turn, OHC stereocilia bundles had formed a V-shaped staircase but with additional inward-pointing "wings" at the open end of the V, thus making them appear more U-shaped (Fig. 1).

At P20, apical OHC hair bundles had formed into a more circular pattern with stereocilia arranged in rows of graded heights (Fig. 2), but the IHC stereo-
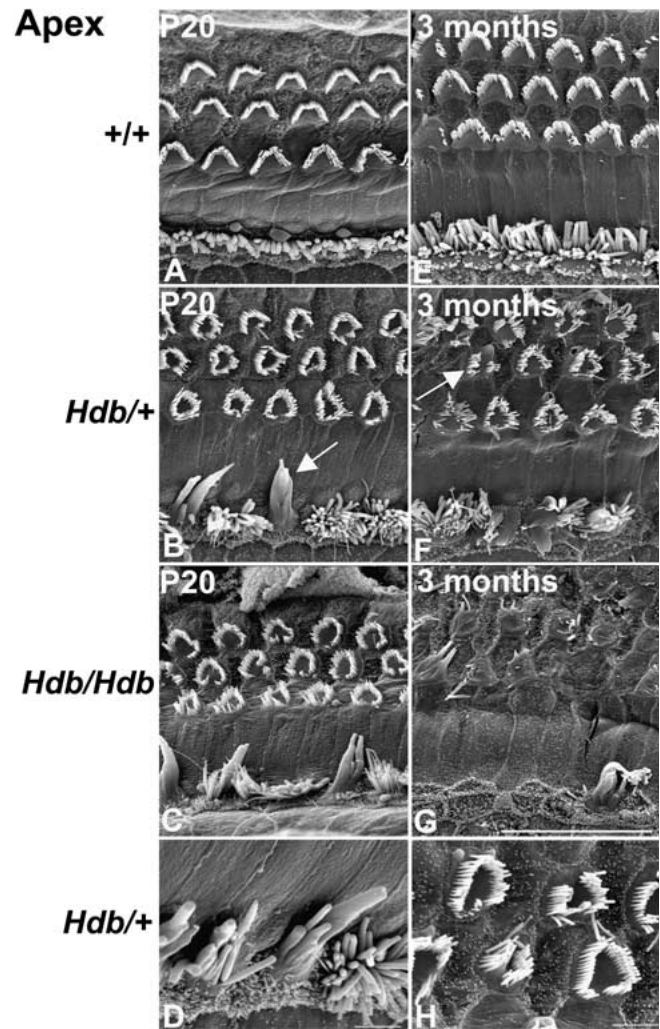

Fig. 2. Scanning electron micrographs of the organ of Corti of P20 and 3-month control (+/+), headbanger heterozygous (*Hdb*/+), and homozygous (*Hdb*/*Hdb*) mice. OHC in the apical coil form O-shaped stereocilia bundles (**B**, **C**, **H**) rather than the normal V-shaped stereocilia bundles seen in the control (**A**). IHC stereocilia have fused into giant stereocilia (**B** arrow, **D**). The IHC fusion is more extensive in the homozygote with many more IHCs affected (**C**). By 3 months, IHC stereocilia fusion is evident in almost all IHCs in the apex in heterozygous mutants (**F**) and signs of stereocilia fusion are seen in the OHCs (**F** arrow). In homozygotes, very few IHC and OHC stereocilia remain in the apex (**G**). Scale bar (**G**) = 10 μm and (**D**, **H**) = 5 μm.

cilia were very disorganized with many additional stereocilia sprouting from each IHC. Many IHC stereocilia had fused together and elongated forming abnormal giant stereocilia (Fig. 2). In older *Hdb*/+ mutant mice (3 months), the process of IHC fusion was progressing in an apical-to-basal direction along the cochlear duct toward the middle coil. Basal turn hair cell stereocilia at P20 and 3 months appeared comparable to wild-type cochleae (data not shown).

Homozygote phenotype of headbanger mutants (Hdb/Hdb). The viability of the homozygote phenotype was established by intercrossing *Hdb* heterozygote mice and monitoring the subsequent litters for litter size and any behavior disparate from the heterozygotes. The heterozygote breeding pairs (*Hdb*/+ × *Hdb*/+ *n* = 7, number of litters observed *n* = 30, number of offspring *n* = 189) produced litters of comparable size to those from wild-type × *Hdb*/+ breeding pairs (*Hdb*/+ × +/+ *n* = 22, number of litters observed *n* = 119, number of mice *n* = 733), suggesting that the pups were not dying *in utero*. The average number of pups per litter from *Hdb*/+ × *Hdb*/+ was 6.3 ± 0.25 compared with 6.2 ± 0.52 from *Hdb*/+ × +/+ breeding pairs and there was no significant difference between the two groups (two-tailed Student's test, *p* = 0.80, *df* = 9.20, *p* < 0.05).

Monitoring of the home-cage behavior of the litters from heterozygote breeding pairs following weaning (P18–21) revealed some pups that displayed increased head bobbing and appeared more hyperactive than their other mutant siblings. Genotyping of these litters (see Methods) confirmed that the more hyperactive mice were homozygous for a candidate mutation, and SEM analyses of the organ of Corti of these mice revealed a more advanced phenotype compared to the heterozygote phenotype as described above. At P20 in *Hdb/Hdb* mice, IHC stereocilia fusion had progressed from the apical to the middle coil such that the P20 homozygote phenotype resembled the 3-month heterozygote phenotype (Fig. 2 and data not shown).

Auditory physiology of the cochlea. *Hdb* mutants display a strong Preyer reflex (ear flick) to a 20-kHz 90-dB-SPL tone burst, suggesting that they do not have a severe or profound hearing loss. However, to determine more accurately the level of hearing in headbanger mutants, we measured compound action potential (CAP) thresholds from the round window of the cochlea, which reflect the synchronous activity of the cochlear nerve neurons. These measures revealed a large increase in CAP thresholds at the low frequencies (3–12 kHz) in *Hdb* heterozygous mice of up to 40 dB (Fig. 3). *Hdb* homozygous mice showed increased CAP thresholds across all frequencies (Fig. 3). These data suggest that the *Hdb* mutation affects hair cell function first in the cochlear apex, consistent with our SEM analyses of *Hdb* cochleas. The endocochlear potentials were recorded in wild-type, *Hdb*/+, and *Hdb/Hdb* animals resulting in mean values of 98.5 ± 2.03 mV, 98.5 ± 2.14 mV, and 98.5 ± 3.50 mV, respectively, which are all within the normal range suggesting that the stria vascularis was functioning normally in *Hdb* animals.
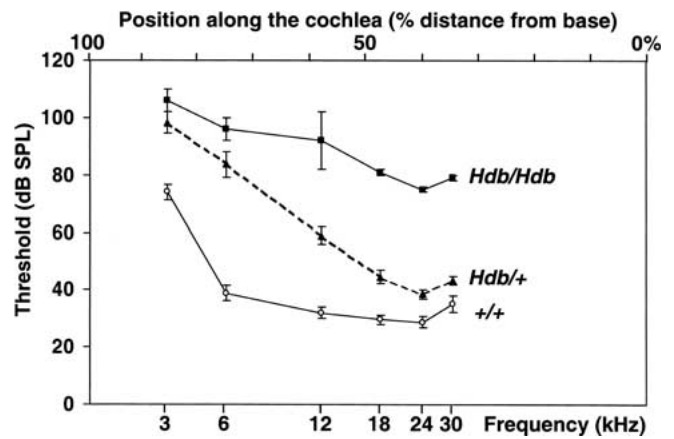
Fig. 3. Compound action potential thresholds from wild-type littermate controls (solid line, open circles ± SEM; *n* = 6), *Hdb* heterozygotes (dashed line, filled triangles ± SEM; *n* = 11), and *Hdb* homozygotes (solid line, black squares ± SEM; *n* = 2) aged 20–23 days, showing that thresholds were raised at the low frequencies (3–12 kHz) in *Hdb* heterozygous mice and across all of the frequencies in *Hdb* homozygous mice. Scale at the top represents frequency place map of cochlear duct (after Ehret 1975).

Defects in the vestibular system of headbanger mutants. Mice with vestibular dysfunction commonly present with abnormal inner ear morphology. Such defects are easily identified by injecting a solution of white paint into the endolymphatic space of the membranous inner ear. This procedure was performed on headbanger heterozygotes and littermate controls. However, all three semicircular canals and ampullae, the utricle and saccule, and all other inner ear features appeared normal at all ages studied (E16.5 +/+ *n* = 12, *Hdb*/+ *n* = 15; P3 +/+ *n* = 4, *Hdb*/+ *n* = 5; P20 +/+ *n* = 8, *Hdb*/+ *n* = 10) (data not shown). The genotypes of these mice were confirmed using the PCR approach as described in the Methods section.

In addition, the sensory organs of the vestibular system were analyzed by SEM to determine if there was any defect that may account for the headbanger behavior. Utricles from *Hdb* heterozygote and wild-type controls at P20 and 5 months were analyzed (P20 +/+ *n* = 6, *Hdb*/+ *n* = 12; 5 months +/+ *n* = 2, *Hdb*/+ *n* = 4). The utricle is composed of type I and type II hair cells. These cell types are distinguished by the length of their kinocilia. The kinocilia of type I cells are of equal length to the tallest of the stereocilia but in type II hair cells the kinocilia are longer than the stereocilia. Both type I and type II cell types were readily identified in both age groups in wild-type utricles. However, *Hdb* heterozygote utricles displayed bundles of very long and thin stereocilia without the normal staircase arrangement, making it difficult to distinguish between the cell types. At

P20, the long stereocilia bundles appeared relatively rigid and perpendicular to the utricle surface, but, at 5 months, the rigidity appeared to have diminished and the stereocilia bundles were splayed and lay against the utricular surface (Fig. 4). The mutant stereocilia also appeared to be longer at 5 months of age than at P20, and often showed wispy ends. Fusion of the stereocilia (as observed in the cochlea) was not seen at these ages in the utricle.
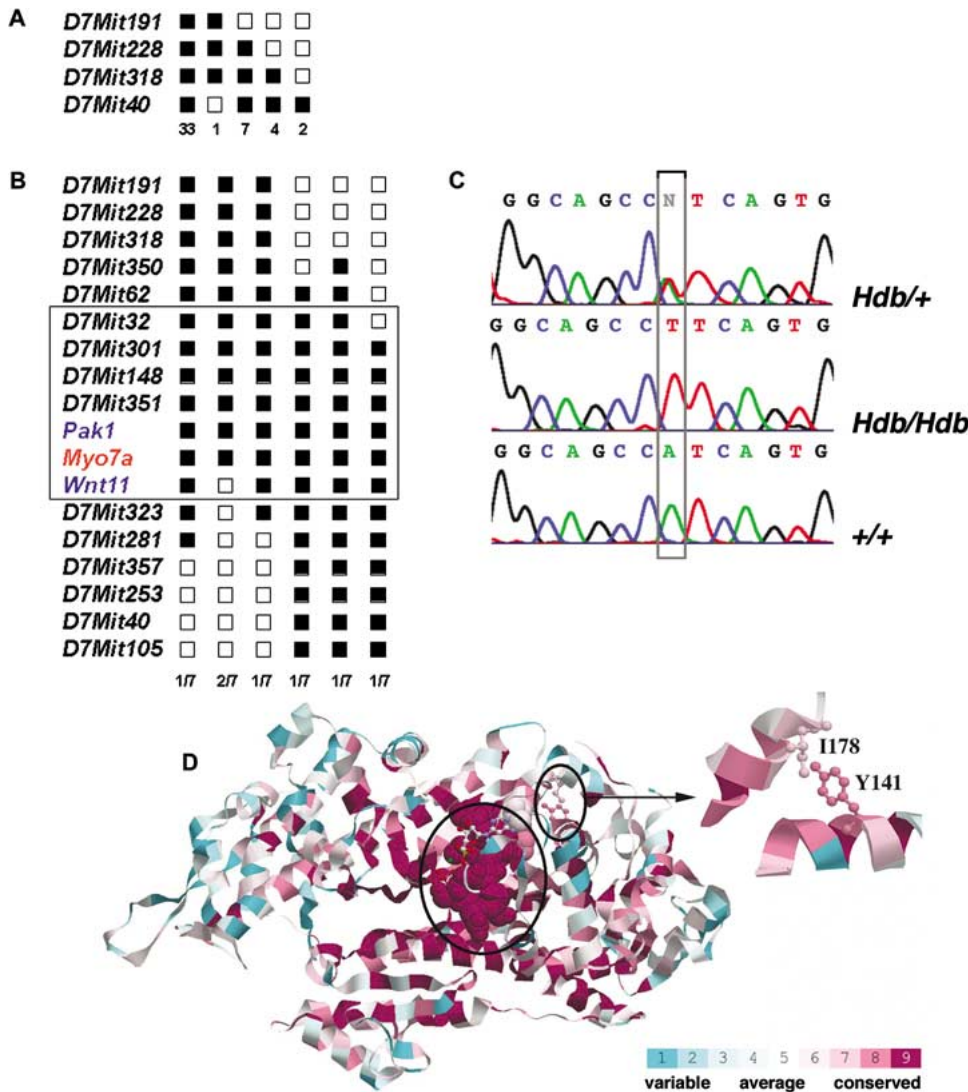
Mapping of the headbanger mutation to Chromosome 7. From the backcross, 71 mice out of 282 N2 progeny were clearly identified as *Hdb* mutants by their abnormal behavior. Using a panel of 59 markers polymorphic between C3HeB/FeJ and C57BL/6J to type 47 of the N2 mutant progeny, a region of linkage to Chromosome 7 was identified between the markers *D7Mit318* and *D7Mit40* (Fig. 5A). No other regions of linkage were found on any of the other autosomes (data not shown). Extending the analysis to all N2 mutant mice and using additional polymorphic markers revealed seven mice with recombinations in the region of the mutation, narrowing the region to 3.3 cM–MIT [Massachusetts Institute of Technology/Whitehead Institute Center for Genome Research (MIT)] (Fig. 5B). Because there were no more mice with recombinations in the region to further narrow the critical region, a screen for mutations was begun in genes located in the linkage interval. We chose to initiate our mutation screen by direct sequencing of the PCR products of homozygote and wild-type cDNAs of *Myo7a* (described below) and p21/cdc42/rac1 activated kinase 1 (*Pak1*) and the genomic sequence of wingless-related MMTV integration site 11 (*Wnt11*). No mutations were found in the cDNA of *Pak1* or the exon sequence and intron–exon boundaries of *Wnt11*. However, a SNP polymorphic between C3HeB/FeJ and C57BL/6J was identified in the *Wnt11* 5′ UTR and subsequently further narrowed down the linkage interval.

Mutation screening of **Myo7a.** The unconventional myosin VIIa is a member of the myosin superfamily of actin-based molecular motors. It has been shown to be essential for normal hair cell development and is involved in deafness and vestibular dysfunction in shaker1 mice (Gibson et al. 1995), as well as in nonsyndromic deafness and Usher syndrome type 1B in humans (Weil et al. 1995). Furthermore, it is expressed in hair cells, and shaker1 mutants show stereocilia bundle defects (Self et al. 1998). For these reasons, the *Myo7a* gene was considered a strong candidate for *Hdb*. Sequence analysis of *Myo7a* cDNA revealed an A531T transversion
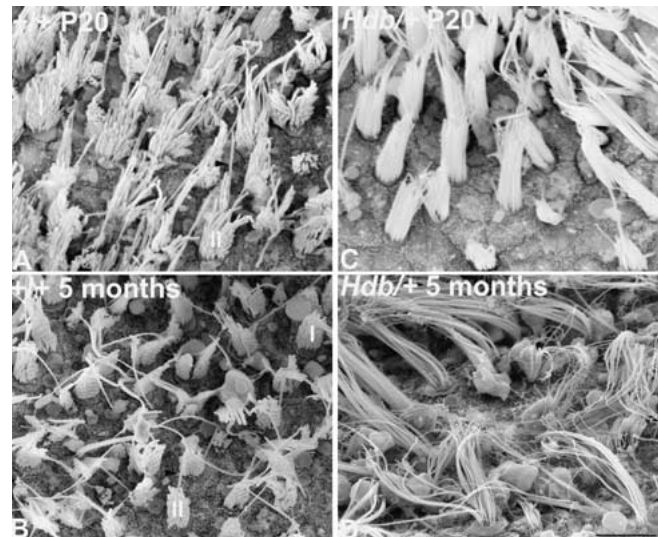
Fig. 4. Scanning electron micrographs taken from control and *Hdb* heterozygote utricles at P20 (**A**, **C**) and 5 months (**B**, **D**). At P20, *Hdb* utricle hair cell stereocilia were very long and thin and lacked the regular height gradation seen in the control (compare **A**, +/+ and **C**, *Hdb*/+). Type I and type II hair cells were therefore difficult to distinguish as defined in the control example (**A**). Type I vestibular hair cells have a staircase array of stereocilia with a kinocilium of equal length to the tallest stereocilia. Type II hair cells, by contrast, have a longer kinocilium extending above the tallest stereocilia (+/+, **A**, **B**). By 5 months, the rigidity in the stereocilia bundles seen at P20 was absent and the stereocilia bundles were splayed and lay against the utricular surface (**D**). Scale bar = 10 μm.

in exon 6 of the gene (Fig. 5C). This mutation was found in headbanger heterozygote and homozygote genomic DNA and cDNA but not in wild-type C3HeB/FeJ, C57BL/6J, *Mus spretus*, and *Mus castaneus* genomic DNA. The mutation was confirmed by reverse sequencing of new mutant cDNA and by direct sequencing of wild-type and homozygote and heterozygote mutant DNA, as well as by the restriction digestion approach used for genotyping as described in the Methods section (data not shown). To date, the *Myo7a* A531T mutation has segregated with the mutant phenotype in all mice tested on the original C3HeB/FeJ genetic background and in clearly affected mice from the backcross (*n* = 278). The mutation is predicted to cause a codon change of ATC to TTC, resulting in an isoleucine-to-phenylalanine amino acid substitution (I178F) of a conserved residue in the head domain of the protein, behind the ATP-binding pocket (Fig. 5D). The degree of conservation of the amino acids among 75 myosin homologs was calculated using ConSurf (http://consurf.tau.ac.il/: (Glaser et al. 2003), which uses the Rate4Site algorithm for estimating the evolutionary rates at each amino acid site. According to

Fig. 5. Headbanger chromosomal localization and *Myo7a* mutation. (**A**) Haplotype figure demonstrates low-resolution mapping of 47 mice that determined Chromosome 7 localization for *Hdb*. (**B**) Haplotype panel shows further genotyping on 7 informative recombinant mice of all N2 mutant mice phenotyped and genotyped. *Hdb* lies between the marker *D7Mit32* and the *Wnt11* gene (outlined). The critical region for the *Hdb* gene is within 8.6 Mb, based on the UCSC Genome Browser, mouse October 2003 assembly (http://www.genome.ucsc.edu). Black boxes denote C3H-type markers and white boxes denote C57BL/6-type markers on the F1-derived chromosome. Genes sequenced without any identified mutations are marked in blue. An A-to-T transversion was found in the *Myo7a* gene (red). (**C**) Sequencing of *Myo7a* showing an A531T transversion in exon 6 in the motor domain of the gene (boxed region). Control cDNA (+/+) shows a single A peak, homozygote cDNA (*Hdb/Hdb*) shows a single T peak, and heterozygote cDNA (*Hdb/+*) shows two peaks of A and T. (**D**) Partial ribbon representation of a 3D model of the myosin VIIa motor domain. The model was obtained using the experimentally determined structure of *Dictyostelium discoideum* myosin IE as a template (Kollmar et al. 2002). The degree of conservation was analyzed using ConSurf (http://consurf.tau.ac.il/; Glaser et al. 2003); residue conservation scores, calculated using 75 homologous sequences, are color coded onto the structure of myosin VIIa (see key). The Mg, ADP, and VO_4 (ball-and-stick) are located in the ATP-binding site (circled; space-filled; maroon), with the mutated I178 and Y141 at the rear (circled; ball-and-stick; shown in inset).

the ConSurf analysis, the isoleucine at position 178 is a conserved residue with a grade of 7 (out of 9; color-coded as pink, see key in Fig. 5D). A CLU-STALW (http://www.ebi.ac.uk/clustalw/) multiple sequence alignment (MSA) of all myosin VIIA molecules identified to date (*Mus musculus*, *Homo sapiens*, *Sus scrofa*, *Rattus norvegicus*, *Brachydanio*

rerio, *Drosophila melanogaster*, *Caenorhabditis elegans*, *Morone saxatilis*; http://www.ncbi.nlm.nih.gov/entrez/) revealed that all had an isoleucine at this position, other than *Patinopecten yessoensis* (valine), *Strongylocentrotus purpuratus* (valine), *Anopheles gambiae* (threonine), and *Dictyostelium discoideum* myosin VIIA (arginine) (data not shown).

Myosin VIIa protein expression and localization in the headbanger mouse cochlea. To investigate whether the mutation identified in *Myo7a* in *Hdb* mutants affected myosin VIIa protein expression, a Western blot was performed on protein extracted from P4 cochleae from a *Hdb*/+ × *Hdb*/+ cross on a C3HeB/FeJ genetic background. A reduction in the levels of myosin VIIa in *Hdb*/+ and *Hdb*/*Hdb* mice was found when compared with the wild-type mice ($p < 0.001$ and 0.01, respectively) (Fig. 6A, Table 1). Antibodies specific to myosin VI and VIIa were used (Hasson et al. 1997) (Fig. 6A). This result does not change whether the protein amounts are normalized versus myosin VI, a hair cell–specific protein marker control, or tubulin, used as a general loading control (Table 1). No significant changes were observed in the levels of myosin VI, indicating that the observed reduction in myosin VIIa protein levels is unique and does not result from a general loss of hair cells.

In order to examine whether the mutant myosin VIIa manages to localize to the cellular locations of its wild-type counterpart, we examined myosin VIIa expression by immunohistochemistry. Myosin VIIa protein localization was unchanged in the headbanger mouse mutants (Fig. 6B).

Complementation test between shaker1 and headbanger. To investigate whether the mutation identified in *Myo7a* in *Hdb* mutants was the causative mutation, a complementation test was performed between a headbanger homozygote mutant and a shaker1 heterozygote. Shaker1 (*sh1/sh1*) mice have a recessive mutation of *Myo7a* and display typical shaker–waltzer-type behavior: deafness, hyperactivity, head tossing, and circling. Heterozygotes (+/*sh1*) have no abnormal phenotype and are comparable to wild-type animals. The allele selected to use for the complementation analysis was *Myo7a*[4626SB]. This allele is associated with very low levels (less than 1% of normal) of myosin VIIa protein, suggesting that it is effectively a null allele (Hasson et al. 1997). *Myo7a*[4626SB]/*Myo7a*[4626SB] homozygotes display disorganized stereocilia bundles that progressively form clumps rather than the ordered V-shaped arrays (Holme and Steel 2002). By P20, many stereocilia bundles have degenerated.
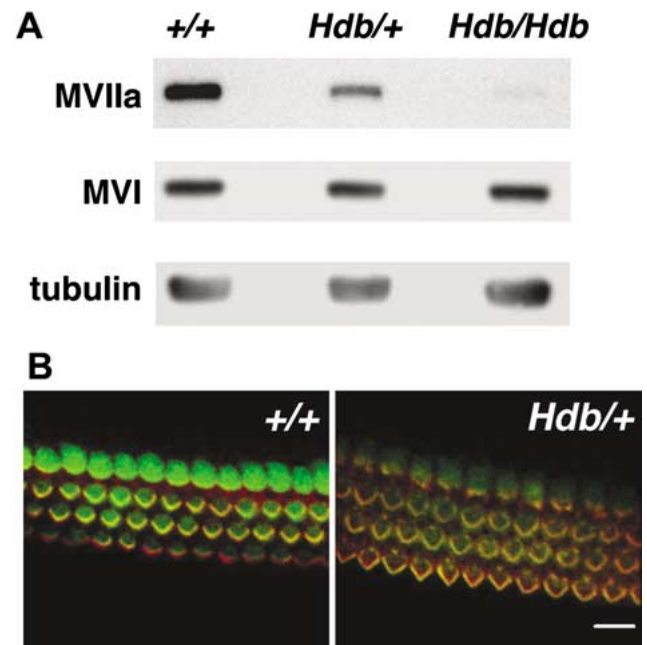
Fig. 6. Myosin VIIa is downregulated in headbanger cochlea, with no change in localization. (**A**) Western blot analysis of cochlea derived from wild-type, *Hdb* heterozygote, and *Hdb* homozygote mice. Antibodies against myosin VIIa showed a reduction in expression, as opposed to myosin VI (a hair cell–specific protein) and tubulin (control for protein concentration). (**B**) Myosin VIIa is localized to the stereocilia and cytoplasm of cochlear hair cells in both mutant mice and controls. No changes in protein localization were observed between the mutant and wild-type mice or between the homozygote and heterozygote mutants.

Analysis of ten confirmed compound heterozygotes (*Hdb*/*Myo7a*[4626SB]) from the *Hdb*/*Hdb* × +/ *Myo7a*[4626SB] breeding pair showed a phenotype similar to the *Hdb* mutant phenotype but with some minor differences (Fig. 7). The apical turn stereocilia bundles of both IHCs and OHCs appeared more disorganized than in *Hdb*/+, but the phenotype was not as severe as seen in *Hdb* homozygotes. A characteristic feature of the *Hdb* homozygote phenotype was an increase in the IHC stereocilia fusion that had advanced to the middle coil by P20. Therefore, we used this feature to quantify the similarity of the *Hdb*/*Myo7a*[4626SB] phenotype to the *Hdb*/*Hdb* phenotype. Hair cell counts (P20–21 +/+ $n = 5$, *Hdb*/+ $n = 7$, *Hdb*/*Hdb* $n = 3$, *Hdb*/*Myo7a*[4626SB] $n = 7$) of

Table 1. Reduction in levels of myosin VIIa, as measured from Western blot by densitometry[a]

|	Wild type	Hdb heterozygote[b]	Hdb homozygote[b]
Myosin VIIa/tubulin	100%	41.16% (13.9)**	25.5% (25.5)*
Myosin VIIa/myosin VI	100%	42.7% (6.9)**	26.6% (18.6)*
Myosin VI/tubulin	100%	93% (18)	90% (32)

[a]The numbers represent an average of three independent experiments. Numbers in parentheses represent one standard deviation.
[b]* and ** represent Student's *t*-test result showing a downregulation versus wild type with a *p* value <0.01 and 0.001, respectively.
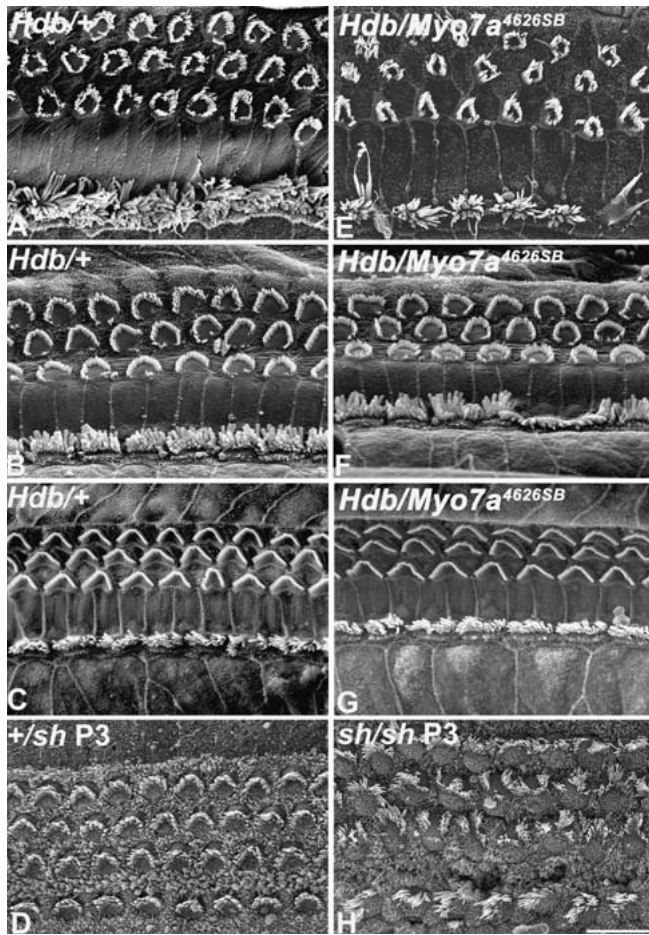
Fig. 7. Scanning electron micrographs taken from the apex (**A**, **E**), the middle (**B**, **F**), and the base (**C**, **G**) of *Hdb* heterozygotes (*Hdb/+*) and compound heterozygotes (*Hdb/Myo7a^{4626SB}*) from a complementation test between *Hdb* and *sh1* mutants. IHC fusion was evident predominantly in the apical coil of compound heterozygote cochleae (**E**); however this was not as frequent as seen in the *Hdb/Hdb* cochlea. OHC stereocilia bundles formed into irregular V and O shapes in the apical (**E**) and the middle (**F**) coils. IHC stereocilia bundles in the middle (**F**) and basal (**G**) coils appeared comparable to controls (**B** and **C**, respectively) with very few fused bundles. The *Hdb/Myo7a^{4626SB}* hair cell phenotype did not resemble the *sh1/sh1* phenotype (compare **H** and **E** apical coil). P3 *sh1* samples are shown in this example rather than adults, because hair cells degenerate rapidly making comparison with the *Hdb* phenotype difficult (**D**, *+/sh* litter mate control). Scale bar = 10 μm.

the apical coil revealed significantly reduced IHC fusion in *Hdb/Myo7a^{4626SB}* compared with *Hdb/Hdb* (*Hdb/Myo7a^{4626SB}* total number of fused IHCs = 1.35/100 ± 0.28 μm; *Hdb/Hdb* total number of fused IHCs = 16.5/100 ± 0.4 μm), suggesting that the phenotype of *Hdb/Myo7a^{4626SB}* and *Hdb/Hdb* was not similar with respect to the IHC stereocilia fusion. Interestingly, the counts revealed no significant difference in the IHC stereocilia fusion between *Hdb/Myo7a^{4626SB}* and *Hdb/+* (*Hdb/+* total number of
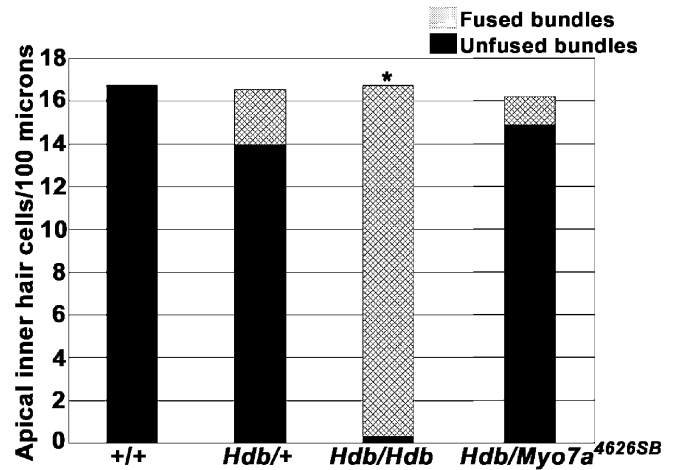
Fig. 8. Hair cell counts of IHC stereocilia fusion of the apical coil from a complementation test between *Hdb* and *sh1* mutants revealed no significant difference in IHC stereocilia fusion between compound heterozygotes (*Hdb/Myo7a^{4626SB}*) and *Hdb* heterozygotes (*Hdb/+*). The amount of IHC stereocilia fusion in the apical coil was significantly greater in *Hdb* homozygote (*Hdb/Hdb*) cochleae compared with all other genotypes (*+/+*, *Hdb/+*, *Hdb/Myo7a^{4626SB}*). Counts were taken from the apex (80%–100% from the base) of between 500 and 800 μm per cochlea (P20–21 *+/+* n = 5, *Hdb/+* n = 7, *Hdb/Hdb* n = 3, *Hdb/Myo7a^{4626SB}* n = 7; *p < 0.01; Student's two-tailed *t*-test between *Hdb/Hdb* and *Hdb/+*, *Hdb/Hdb* and *Hdb/Myo7a^{4626SB}*, and *Hdb/Hdb* and wild-type controls).

fused IHCs = 2.61/100 ± 0.64 μm), suggesting that the compound heterozygote phenotype resembled the *Hdb* heterozygote phenotype more than the *Hdb* homozygote phenotype with respect to the IHC stereocilia fusion (Fig. 8). IHC stereocilia fusion was also predominant in the apical coil of *Hdb/Myo7a^{4626SB}* cochleae, with only random two or three fused IHC stereocilia bundles seen in the middle coil. This is in contrast to the extensive IHC stereocilia bundle fusion observed in the middle coil of *Hdb/Hdb* cochleae. In addition, the compound heterozygote phenotype did not show any similarity to the *Myo7a^{4626SB}* homozygote phenotype (Fig. 7). Thus, we found no evidence of noncomplementation, suggesting either that the *Myo7a* mutation detected in headbanger does not cause the pathology, that the different nature of the mutations in the two alleles led to them not acting in a simple additive manner, or that the mixed genetic background of the compound heterozygotes confounded the observations (see Discussion).

Discussion

Our findings indicate that the headbanger gene is involved in stereocilia development and mainte-

nance. At the earliest age analyzed (E18.5), the arrangement of the stereocilia bundle is abnormal. In the apex of the cochlea, the stereocilia bundles are of a relatively uniform length and extend from the whole apical surface of the hair cell rather than forming the regular staircase array seen in controls. In the base of the cochlea, OHC stereocilia often form a U-shaped bundle rather than the normal V-shape bundle. In addition, apical IHC stereocilia fuse and form giant, elongated bundles that eventually degenerate. This phenotype is in contrast to that of shaker1 mice that carry a null mutation in *Myo7a*. Shaker1 stereocilia are found grouped together in clumps at the top of the hair cell and are uniformly affected throughout the cochlea, with very few stereocilia bundles remaining by P20 (Self et al. 1998). Genetic mapping localized the *Hdb* mutation to the same chromosomal interval as *Myo7a*, and all 278 *Hdb* mutant mice identified by their abnormal behavior to date have carried the A531T mutation, demonstrating that the mutation always segregated with the mutant phenotype. An important question we wished to ask was whether the mutation identified in the motor domain of *Myo7a* in *Hdb* mice is responsible for their phenotype.

The *Hdb* mutation is predicted to lead to an isoleucine-to-phenylalanine amino acid substitution (I178F). I178 is in close proximity to the P-loop, a segment of the nucleotide ATP-binding site (consensus sequence GESGAGKT) (Fig. 5D). Isoleucine is a branched, aliphatic amino acid, whereas phenylalanine has a much larger aromatic side chain that may cause steric hindrance and lead to structural destabilization of the protein. For example, based on the 3D model we derived, a highly conserved tyrosine at position 141 would be in close proximity to the mutated phenylalanine and appears to be in an unfavorable conformation. Favorable π–orbital interactions between aromatic rings are formed by parallel stacking of the aromatic rings, which may now occur with the *Hdb* mutation and cause a change of conformation in the myosin VIIa protein.

In the inner ear, myosin VIIa is expressed in the cytoplasm, and, in particular, along the entire length of the stereocilia, the cuticular plate, and the pericuticular necklace (Hasson et al. 1997). This suggests that it may perform a function during the development of the stereocilia consistent with the hair cell pathology observed in mutants like shaker1 and headbanger. Myosin VIIa expression levels were substantially reduced in both heterozygote and homozygote headbanger cochlea, although localization did not appear to be affected.

Hdb is a dominant mutation and to date only recessive mutations in *Myo7a* in mice have been

identified. This is somewhat surprising since myosin VIIA is thought to form a dimer because of the presence of a predicted coiled-coil structure (Hasson et al. 1995; Weil et al. 1996, 1997), and dimers may be disproportionately affected by the presence of one copy of a mutant gene. A 9-bp deletion affecting the coiled-coil region of *MYO7A* has been reported (Liu et al. 1997b), resulting in a moderate, progressive, postlingual, nonsyndromic hearing loss with high frequencies affected more than low frequencies (Tamagawa et al. 2002). Interestingly, a second dominant *MYO7A* mutation has been found in a family with progressive hearing loss affecting low frequencies first. Genetic linkage analysis placed the locus at human Chromosome 11 in the region containing *MYO7A*, and subsequent mutation analysis revealed a missense mutation affecting the motor domain (Street et al. 2004). More than 80 pathological *MYO7A* mutations have been reported in human USH1B families but no other mutations have been identified with dominant inheritance (Levy et al. 1997; Liu et al. 1997a,b; Weil et al. 1997; Astuto et al. 2002). The identification of dominant mutations in the human *MYO7A* gene highlights the fact that dominant pathological mutations could exist in mouse *Myo7a*. Furthermore, the similarity in the low-frequency pattern of hearing loss in a human family with a missense mutation affecting the motor domain and the predominantly low-frequency impairment in headbanger heterozygotes supports the suggestion that the *Myo7a* mutation in headbanger could potentially be the causative mutation. It is clearly important to improve our understanding of the molecular basis of human hearing impairment, as this is a prerequisite for developing treatments, and the availability of a range of mouse mutations with features similar to those seen in human hearing impairment will facilitate this process.

Despite these factors that support the notion that *Myo7a* may be involved in the *Hdb* phenotype, several aspects of our data are difficult to explain if the *Myo7a* mutation in *Hdb* mice is responsible for their phenotype. The stereocilia defects observed in *Hdb* mutants are quite different than the stereocilia defects seen in shaker1 mutants. OHC stereocilia of headbanger mutants show ectopic stereocilia giving an O-shaped or U-shaped appearance, a feature that is not seen in any of the ten shaker1 alleles examined so far (Self et al. 1998; Holme and Steel 2002). There is an apex to base progression of severity in *Hdb* mutants in contrast to the base to apex gradient seen in shaker1 mice, and the extensive IHC fusion observed in *Hdb* IHCs is not generally seen in any other *Myo7a* mutant. If headbanger is an allele of

Myo7a, how can we account for the phenotypic differences observed between the other known *Myo7a* alleles and *Hdb*? The headbanger colony is maintained on a C3HeB/FeJ genetic background. In contrast, most of the shaker1 alleles (including *Myo7a*^{4626SB}) are maintained on a mixed CBA/BS genetic background (Libby and Steel 2001). The different genetic backgrounds of each mutant line may influence the effects that the mutation in *Myo7a* has on the resulting phenotype in shaker1 and headbanger mutants, resulting in the observed disparity between the two phenotypes.

Indeed, preliminary studies have shown that when *Hdb* mice are outcrossed to the CBA/Ca genetic background, their behavioral phenotype is ameliorated and it becomes difficult to identify mutant animals (unpublished observations). Moreover, only 71 of the 282 N2 headbanger mice showed a clear phenotype that allowed us to include them in the genome scan. This suggests that there may be a modifier in the C3HeB/FeJ genetic background that aggravates the mutation in *Hdb*.

An alternative explanation for the differences seen between *Hdb* and *sh1* mutants is that they could be due to the type of mutation. Headbanger is a dominant mutation and shaker1 is recessive. At least two of the shaker1 alleles appear to be null alleles because no myosin VIIa protein could be detected (Hasson et al. 1997), which suggests that any dominant *Myo7a* mutation is unlikely to act by haploinsufficiency. If the *Myo7a* mutation underlies the *Hdb* phenotype, the mechanism of action of the *Hdb* mutation may be very different; for example, it may have a dominant negative effect or gain of function. Moreover, the ENU mutagenesis may lead to additional induced base changes within the linked region which would cause the *Hdb* phenotype. Should this be the case, the mutant product may interact with or transcriptionally regulate myosin VIIA, leading to reduction of expression levels in this myosin.

To investigate whether the mutation identified in *Myo7a* in *Hdb* mutants was indeed responsible for the *Hdb* pathology, a complementation test was performed between *Hdb/Hdb* and +/*sh1* mice. If the resulting phenotype in the compound heterozygote animals was the same as the *Hdb/Hdb* phenotype, then this information would support the *Myo7a* mutation in *Hdb* as being the causative mutation. However, the compound heterozygote phenotype resembled more closely the *Hdb/+* heterozygote phenotype rather than the *Hdb/Hdb* phenotype and had no similarities to the *sh1/sh1* phenotype. This result suggests that the *Myo7a* mutation in *Hdb* has a different mode of action than in the shaker1 alleles

or that a different gene may be responsible for the *Hdb* pathology. In conclusion, we have demonstrated that the *Hdb* locus encodes a protein required for the normal arrangement and growth of the stereocilia bundle on hair cells in the organ of Corti and in the vestibular system and represents a new dominant mouse mutant with a novel hair cell phenotype.

Furthermore, we describe a *Myo7a* mutation that cosegregates with the *Hdb* phenotype and may or may not be the causative factor for the low-frequency hearing loss and vestibular dysfunction in headbanger mice. A duplication of the mutation by transgenesis and functional analysis, such as motility assays, will aid in determining whether *Myo7a* or another gene underlies the headbanger mutant phenotype.

References

1. Ahmed AM, Riazuddin S, Bernstein SL, Ahmed Z, Khan S, et al. (2001) Mutations of the protocadherin gene *PCDH15* cause Usher syndrome type 1F. Am J Hum Genet 69, 25–34

2. Alagramam KN, Murcia CL, Kwon HY, Pawlowski KS, Wright CG, Woychik RP (2001) The mouse Ames Waltzer hearing-loss mutant is caused by mutation of *Pcdh15*, a novel protocadherin gene. Nat Genet 27, 99–102

3. Astuto LM, Kelley PM, Askew JW, Weston MD, Smith RJ, et al. (2002) Searching for evidence of DFNB2. Am J Med Genet 109, 291–297

4. Bolz H, von Brederlow B, Ramirez A, Bryda EC, Kutsche K, et al. (2001) Mutation of CDH23, endocding a new member of the cadherin gene family, cause Usher syndrome type 1D. Nat Genet 2001 27, 108–112

5. Curtin JA, Quint E, Tsipouri V, Arkell RM, Cattanach B, et al. (2003) Mutation of *Celsr1* disrupts planar polarity of inner ear hair cells and causes severe neural tube defects in the mouse. Curr Biol 13, 1129–1133

6. Di Palma F, Holme RH, Bryda EC, Belyantseva IA, Pellegrino R, et al. (2001) Mutations in *Cdh23*, encoding a new type of cadherin, cause stereocilia disorganization in waltzer, the mouse model for Usher syndrome type 1D. Nat Genet 27, 103–107

7. Donaudy F, Ferrara A, Esposito L, Hertzano R, Ben-David O, et al. (2003) Multiple mutations of *MYO1A*, a cochlear-expressed gene, in sensorineural hearing loss. Am J Hum Genet 72, 1571–1577

8. Ehret G (1975) Masked auditory thresholds, critical ratios, and scales of the basilar membrane of the housemouse (*Mus musculus*). J Comp Physiol 103, 329–341

9. Erven A, Skynner MJ, Okumura K, Takebayashi S, Brown SD, et al. (2002) A novel stereocilia defect in sensory hair cells of the deaf mouse mutant Tasmanian devil. Eur J Neurosci 16, 1433–1441

10. Gibson F, Walsh J, Mburu P, Varela A, Brown KA, et al. (1995) A type VII myosin encoded by the mouse deafness gene shaker-1. Nature 374, 62–64

11. Glaser F, Pupko T, Paz I, Bell RE, Bechor–Shental D, et al. (2003) ConSurf: identification of functional regions in proteins by surface-mapping of phylogenetic information. Bioinformatics 19, 163–164

12. Hasson T, Heintzelman MB, Santos–Sacchi J, Corey DP, Mooseker MS (1995) Expression in cochlea and retina of myosin VIIa, the gene product defective in Usher syndrome type 1B. Proc Natl Acad Sci USA 92, 9815–9819

13. Hasson T, Walsh J, Cable J, Mooseker MS, Brown SD, et al. (1997) Effects of shaker-1 mutations on myosin-VIIa protein and mRNA expression. Cell Motil Cytoskeleton 37, 127–138

14. Holme RH, Steel KP (2002) Stereocilia defects in waltzer (*Cdh23*) shaker1 (*Myo7a*) and double waltzer/shaker1 mutant mice. Hear Res 169, 13–23

15. Hrabé de Angelis MH, Flaswinkel H, Fuchs H, Rathkolb B, Soewarto D, et al. (2000) Genome-wide, large-scale production of mutant mice by ENU mutagenesis. Nat Genet 25, 444–447

16. Kaltenbach JA, Falzarano PR, Simpson TH (1994) Postnatal development of the hamster cochlea. II. Growth and differentiation of Stereocilia bundles. J Comp Neurol 350, 187–198

17. Kelley MW, Xu XM, Wagner MA, Warchol ME, Corwin JT (1993) The developing organ of Corti contains retinoic acid and forms supernumerary hair cells in response to exogenous retinoic acid in culture. Development 119, 1041–1053

18. Kiernan AE, Zalzman M, Fuchs H, de Angelis MH, Balling R, et al. (1999) Tailchaser (*Tlc*): a new mouse mutation affecting hair bundle differentiation and hair cell survival. J Neurocytol 28, 969–985

19. Kollmar M, Durrwang U, Kliche W, Manstein DJ, Kull FJ (2002) Crystal structure of the motor domain of a class-I myosin. EMBO J 21, 2517–2525

20. Levy G, Levi–Acobas F, Blanchard S, Gerber S, Larget–Piet D, et al. (1997) Myosin VIIA gene: heterogeneity of the mutations responsible for Usher syndrome type IB. Hum Mol Genet 6, 111–116

21. Libby RT, Steel KP (2001) Electroretinographic anomalies in mice with mutations in *Myo7a*, the gene involved in human Usher syndrome type 1B. Invest Ophthalmol Vis Sci 42, 770–778

22. Liu XZ, Newton VE, Steel KP, Brown SD (1997a) Identification of a new mutation of the myosin VII head region in Usher syndrome type 1. Hum Mutat 10, 168–170

23. Liu XZ, Walsh J, Tamagawa Y, Kitamura K, Nishizawa M, et al. (1997b) Autosomal dominant non-syndromic deafness caused by a mutation in the myosin VIIA gene. Nat Genet 17, 268–269

24. Martin P, Swanson GJ (1993) Descriptive and experimental analysis of the epithelial remodellings that control semicircular canal formation in the developing mouse inner ear. Dev Biol 159, 549–558

25. Probst FJ, Fridell RA, Raphael Y, Saunders TL, Wang A, et al. (1998) Correction of deafness in shaker-2 mice by an unconventional myosin in a BAC transgene. Science 280, 1444–1447

26. Self T, Mahony M, Fleming J, Walsh J, Brown SD, et al. (1998) Shaker-1 mutations reveal roles for myosin VIIA in both development and function of cochlear hair cells. Development 125, 557–566

27. Self T, Sobe T, Copeland NG, Jenkins NA, Avraham KB, et al. (1999) Role of myosin VI in the differentiation of cochlear hair cells. Dev Biol 214, 331–341

28. Steel KP, Smith RJ (1992) Normal hearing in Splotch (*Sp/+*), the mouse homologue of Waardenburg syndrome type 1. Nat Genet 2, 75–79

29. Street VA, Kallman JC, Kiemele KL (2004) Modifier controls severity of a novel dominant low frequency myosin VIIA (*MYO7A*) auditory mutation. J Med Genet 41, e62

30. Tamagawa Y, Ishikawa K, Ishida T, Kitamura K, Makino S, et al. (2002) Phenotype of DFNA11: a nonsyndromic hearing loss caused by a myosin VIIA mutation. Laryngoscope 112, 292–297

31. Tilney LG, Tilney MS, DeRosier DJ (1992) Actin filaments, stereocilia, and hair cells: how cells count and measure. Annu Rev Cell Biol 8, 257–274

32. Vreugde S, Erven A, Kros CJ, Marcotti W, Fuchs H, et al. (2002) Beethoven, a mouse model for dominant, progressive hearing loss DFNA36. Nat Genet 30, 257–258

33. Weil D, Blanchard S, Kaplan J, Guilford P, Gibson F, et al. (1995) Defective myosin VIIA gene responsible for Usher syndrome type 1B. Nature 374, 60–61

34. Weil D, Levy G, Sahly I, Levi–Acobas F, Blanchard S, et al. (1996) Human myosin VIIA responsible for the Usher 1B syndrome: a predicted membrane-associated motor protein expressed in developing sensory epithelia. Proc Natl Acad Sci USA 93, 3232–3237

35. Weil D, Kussel P, Blanchard S, Levy G, Levi–Acobas F, et al. (1997) The autosomal recessive isolated deafness, DFNB2, and the Usher 1B syndrome are allelic defects of the myosin-VIIA gene. Nat Genet 16, 191–193

36. Weston MD, Kelley PM, Overbeck LD, Wagenaar M, Orten DJ, et al. (1996) Myosin VIIA mutation screening in 189 Usher syndrome type 1 patients. Am J Hum Genet 59, 1074–1083